IOP Publishing Journal of Physics A: Mathematical and Theoretical

J. Phys. A: Math. Theor. **44** (2011) 175203 (22pp) doi:10.1088/1751-8113/44/17/175203

Inter-particle gap distribution and spectral rigidity of the totally asymmetric simple exclusion process with open boundaries

Milan Krbálek and Pavel Hrabák

Faculty of Nuclear Sciences and Physical Engineering, Czech Technical University in Prague, Prague, Czech Republic

E-mail: milan.krbalek@fjfi.cvut.cz

Received 22 February 2011, in final form 8 March 2011
Published 4 April 2011
Online at stacks.iop.org/JPhysA/44/175203

Abstract

We consider the one-dimensional totally asymmetric simple exclusion process (TASEP model) with open boundary conditions and present the analytical computations leading to the exact formula for distance clearance distribution, i.e. probability density for a clear distance between subsequent particles of the model. The general relation is rapidly simplified for the middle part of the one-dimensional lattice. Both the analytical formulas and their approximations are compared with the numerical representation of the TASEP model. Such a comparison is presented for particles occurring in the internal part as well as in the boundary part of the lattice. Furthermore, we introduce the pertinent estimation for the so-called spectral rigidity of the model. The results obtained are sequentially discussed within the scope of vehicular traffic theory.

PACS numbers: 02.50.−r, 05.45.−a, 89.40.−a

(Some figures in this article are in colour only in the electronic version)

1. Introduction and motivation

The effect of queuing is one of commonly appearing phenomena in nature. It can be disclosed in microbiological systems, societies of animals, computer networks, public transport systems, car parking manoeuvres, and many others. In recent years, queuing has attracted attention of many physicists and mathematicians. It is well known that many of above-mentioned systems belong to the same class of mathematical tasks. A convenient way of investigating such systems in detail can be found in space-discrete and time-continuous one-dimensional models based on asymmetric exclusion processes (ASEP). Indeed, the family of asymmetric exclusion processes is as wide ranging as the family of its applications. Specifically, the ASEP models have been successfully used for the description of protein synthesis [1, 2], polymers in

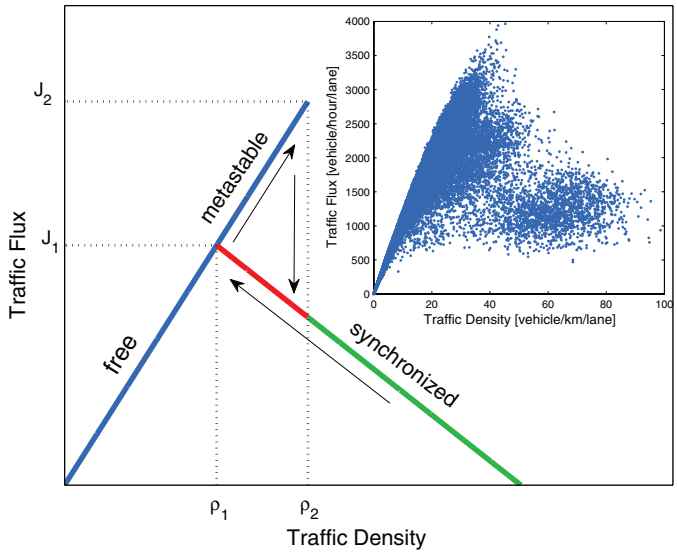

Figure 1. The empirical flow–density relation and relevant schematic representation. The dependence of the traffic flux J on the traffic density ϱ for realistic traffic flows is used to be compared to a mirror image of the Greek letter λ (see [15] or [16]). The relation $J = J(\varrho)$ extracted from the induction-double-loop-detector data is visualized in the inset.

random media [3], fluctuations in shock fronts [4–7], gel electronics [8], in molecular biology [9], and finally in physics of traffic [10–13] or [14].

In this paper, we focus predominantly on those aspects of cellular modeling having a vehicular-traffic interpretation. With respect to the fact that the macroscopical behavior of the totally asymmetric simple exclusion process (TASEP) (represented for example by the fundamental relation between the flux and density of the model) corresponds to that detected in the freeway samples (compare figures 1 and 4 for illustration), it is meaningful to consider the TASEP model as a possible choice for a one-lane traffic simulator. However, besides the confrontation of macroscopic quantities, it is indispensable to make a comparison of microscopic quantities. Recently, extensive investigations of traffic data ([18–23] or [24]) provided a good insight into the microstructure of traffic samples. It has been demonstrated in some of the above-mentioned articles that inter-vehicle gap statistics (clearance distribution) in real-road traffic can be estimated very well by the one-parametric family of functions:

$$\wp(r) = A\Theta(r)\,\mathrm{e}^{-\frac{\nu}{r}}\,\mathrm{e}^{-Br}, \tag{1}$$

where

$$B = \nu + \frac{3 - \mathrm{e}^{-\sqrt{\nu}}}{2}, \tag{2}$$

$$A^{-1} = 2\sqrt{\frac{\nu}{B}}\mathcal{K}_1(2\sqrt{B\nu}). \tag{3}$$

Equation (1) describes an analytical prediction derived for thermal-like traffic gas, whose steady state is in a good consonance with experimental traffic data. We remark that the functions $\Theta(x)$and $\mathcal{K}_\lambda(x)$ represent the Heaviside step-function

$$\Theta(x) = \begin{cases} 1, & x > 0 \\ 0, & x \leqslant 0 \end{cases}$$

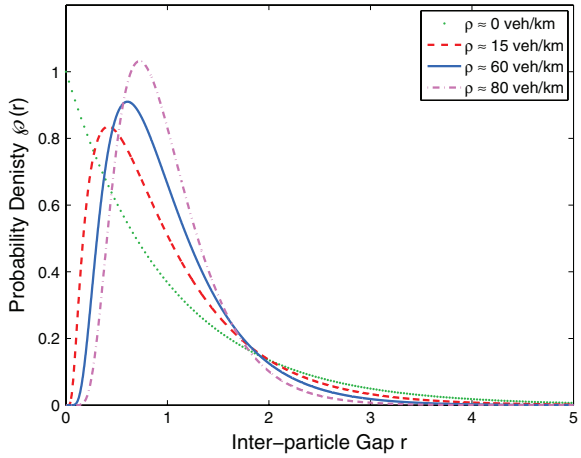

Figure 2. Clearance distribution for real-road traffic. The curves visualize the analytical estimations (1) of the inter-particle statistics obtained for the densities indicated in the legend.

and the modified Bessel's function of the second kind (MacDonald's function), respectively. Furthermore, the distribution $\wp(r)$ fulfills two normalization conditions:

$$\int_{\mathbb{R}} \wp(r)\,\mathrm{d}r = 1 \tag{4}$$

and

$$\int_{\mathbb{R}} r\wp(r)\,\mathrm{d}r = 1. \tag{5}$$

The latter represents a scaling to the mean clearance equal to 1. We add that the one and only parameter ν is related to the traffic density ϱ (see [25] for details). Roughly speaking, such a parameter (called a mental strain coefficient) reflects a rate of psychological pressure which the car drivers are under during driving manoeuvres. The changes of traffic status from free flows to congested flows and vice versa are accompanied by the adequate changes of the mental strain coefficient ν, i.e. by the adequate changes of clearance distribution. The chosen representatives of the relevant analysis are displayed in figure 2. Here, one can detect the basic probabilistic trends of distances among succeeding cars. Whereas in the region of small densities (free traffic regime) the relevant probability density is essentially exponential (which fully corresponds to the fact that cars interactions are negligible), the distribution $\wp(r)$ changes rapidly if congested data are observed. In this case, the stronger mutual interactions among vehicles lead to hardcore repulsions in the system, which results in the fact that $\lim_{r\to 0_+} \wp(r) = 0$. As discussed in [25], the intermediate region of metastable traffic states shows a substantial growth of the parameter ν. This is influenced by the fact that the driver, moving quite fast in relatively dense traffic flow, is under considerable psychological pressure. After the transition from the free to congested regime, the pressure momentarily declines because of a decrease in the mean velocity. Finally, if the traffic flow becomes denser and denser, the mental strain coefficient ν is increasing further. This finally culminates in the creation of stop-and-go traffic waves.

The main goal of this paper is to describe some correspondences between the microstructure of the asymmetric simple exclusion model and real-road traffic. For this purpose, we will compare (in the first part of this work) the relevant clearance distributions,

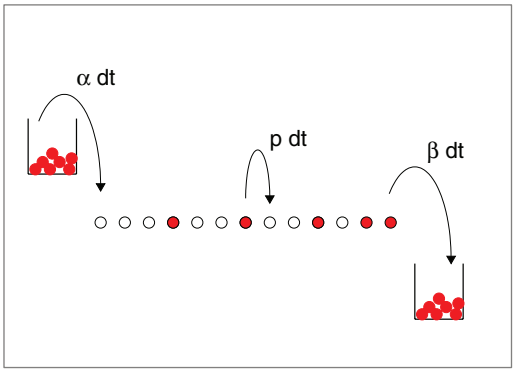

Figure 3. Definition of the TASEP. The configuration visualized can be identified with the vector $\mathcal{C} = (0, 3, 1, 2, 1, 2, 1, 1, 2)$.

i.e. probability densities for clear gap among all pairs of succeeding particles/vehicles. Subsequently we will analyze the associated spectral rigidities of both systems and will discuss their similarities.

2. The TASEP with open boundaries

Consider a chain of length N containing N equivalent cells and define three fixed parameters $\alpha, \beta, p \in [0, 1]$. Let each cell to be either occupied by one particle or empty. During the infinitesimal time interval $\mathrm{d}t$, each particle hops to the immediate site (in the defined direction) with probability $p\mathrm{d}t$ if the target site is empty. In the opposite case (if the target site is occupied), the particle does not change its location. If the first cell ($\ell = 1$) is empty, a new particle is injected into the chain with probability $\alpha\mathrm{d}t$. Similarly, if the last cell ($\ell = N$) is occupied, the relevant particle leaves the chain with probability $\beta\mathrm{d}t$. This definition can be generalized if needed; however, for all purposes the original formulation is fully sufficient. Furthermore, we will use (without loss of generality) the re-scaled variant of the model where $p = 1$.

The sketched rules define a simple driven lattice model of one-lane traffic whose elements are hard-core-repulsed by 'implicit forces' derived from the above-mentioned exclusion rules. A great merit of such a model lies in the exact solvability of the associated steady state. Indeed, two alternative methods for the exact solution of the TASEP are outlined in [26, 27]. For the purpose of this research, we consistently use the methods based on the *matrix formulation* introduced in [27] and elaborated in [28] and [29]. According to this matrix method, we consider the matrices D, E (infinite dimensional, in general) and vectors $\langle w|$ and $|v\rangle$ satisfying the following algebraic rules:

$$DE = D + E, \tag{6}$$

$$\langle w|E = \frac{1}{\alpha}\langle w|, \tag{7}$$

$$D|v\rangle = \frac{1}{\beta}|v\rangle. \tag{8}$$

Although each configuration of the model can naturally be described by the binary sequence

$$\mathcal{T} = (\tau_1, \tau_2, \ldots, \tau_N) \in \{0, 1\}^N,$$

it is profitable to use the following convention. Let the symbol $\mathcal{C} = (n_1, m_1, n_2, m_2, \ldots, n_q, m_q)$ denote the configuration of the TASEP chain such that (starting from the initial cell of the chain) n_1 is the maximal number of occupied cells (i.e. the (n_1+1)st cell is empty), m_1 is the maximal number of empty cells (starting from the (n_1+1)st cell), when the (n_1+m_1+1)st cell is occupied, and so on. Thus, $\sum_i n_i + \sum_j m_j = N$. The previous definition (visualized for lucidity in figure 3) corresponds unambiguously to the relevant arrangement of the particles inside the TASEP chain, which means that there exists some bijection between $\mathcal{T}$ and $\mathcal{C}$. Moreover, it has been proved in [27] that the steady-state probability of an arbitrary configuration $\mathcal{C}$ reads as

$$\mathrm{P}_{\mathrm{ss}}(\mathcal{C}) = \frac{1}{\mathcal{Z}_N} \frac{\langle w| D^{n_1} E^{m_1} D^{n_2} E^{m_2} \cdots |v\rangle}{\langle w|v\rangle}, \tag{9}$$

where the constant $\mathcal{Z}_N$ assures the proper normalization, i.e.

$$\sum_{\mathcal{C}_k} \mathrm{P}_{\mathrm{ss}}(\mathcal{C}_k) = 1$$

for k running over all possible configurations. In fact, such a probability can be calculated directly using relations (6), (7), and (8), i.e. without knowing the specific representation of the matrices D, E and vectors $\langle w|$ and $|v\rangle$. Moreover, let the symbol

$$\omega_{\mathcal{T}}(i) = \begin{cases} 1, & i\text{th site is occupied} \\ 0, & i\text{th site is empty,} \end{cases}$$

represent (for the fixed configuration $\mathcal{T}$) the binary functional $\omega_{\mathcal{T}} : \{1, 2, \ldots, N\} \mapsto \{0, 1\}$. Let the symbol

$$\mathscr{X} = (n_1, m_1, \ell_1, n_2, m_2, \ell_2, \ldots, n_q, m_q, \ell_q)$$

denote the set of all configurations such that n_1 is the maximal number of occupied cells (i.e. the (n_1+1)st cell is empty), m_1 is the maximal number of empty cells (starting from the (n_1+1)st cell), when the (n_1+m_1+1)st cell is occupied, and ℓ_1 is the number of cells (behind the (n_1+m_1)th cell) which can be arbitrarily occupied or not. Precisely speaking, the symbol $\mathscr{X}$ corresponds to the set

$$\begin{aligned}
&\{(\omega_{\mathcal{T}}(1), \omega_{\mathcal{T}}(2), \ldots, \omega_{\mathcal{T}}(N)) \in \{0,1\}^N : \omega_{\mathcal{T}}(1) = \omega_{\mathcal{T}}(2) = \cdots = \omega_{\mathcal{T}}(n_1) = 1 \wedge \\
&\omega_{\mathcal{T}}(n_1+1) = \omega_{\mathcal{T}}(n_1+2) = \cdots = \omega_{\mathcal{T}}(n_1+m_1) = 0 \wedge \\
&\omega_{\mathcal{T}}(n_1+m_1+\ell_1+1) = \omega_{\mathcal{T}}(n_1+m_1+\ell_1+2) = \cdots = \omega_{\mathcal{T}}(n_1+m_1+\ell_1+n_2) \\
&\qquad = 1 \wedge \omega_{\mathcal{T}}(n_1+m_1+\ell_1+n_2+1) = \omega_{\mathcal{T}}(n_1+m_1+\ell_1+n_2+2) = \cdots \\
&\qquad = \omega_{\mathcal{T}}(n_1+m_1+\ell_1+n_2+m_2) = 0 \wedge \\
&\omega_{\mathcal{T}}(n_1+m_1+\ell_1+n_2+m_2+\ell_2+1) = \cdots = \omega_{\mathcal{T}}(n_1+m_1+\ell_1+n_2+m_2+\ell_2+n_3) \\
&\qquad = 1 \wedge \cdots\}.
\end{aligned}$$

As follows from equation (9), the probability for finding the system in one of configurations included in $\mathscr{X}$ is

$$\mathrm{P}_{\mathrm{ss}}(\mathscr{X}) = \frac{1}{\mathcal{Z}_N} \frac{\langle w| D^{n_1} E^{m_1} (D+E)^{\ell_1} D^{n_2} E^{m_2} (D+E)^{\ell_2} \cdots |v\rangle}{\langle w|v\rangle}. \tag{10}$$

As a direct consequence of this assertion (or directly from equation (9)), we easily deduce that the partition sum is of the form (see also [27])

$$\mathcal{Z}_N = \frac{\langle w|(D+E)^N|v\rangle}{\langle w|v\rangle}.$$

For completeness, we note that another way for obtaining this relationship is the generating function approach (see [29]). Using lemma 4 and notation (A.2), we can assert that

$$\mathcal{Z}_N = \frac{1}{\langle w|v\rangle}\sum_{m=1}^{N}\frac{m(2N-m-1)!}{N!(N-m)!}\sum_{i=0}^{m}\langle w|E^i D^{m-i}|v\rangle = \sum_{m=1}^{N}\mathtt{B}_{N,m}\sum_{i=0}^{m}\frac{1}{\alpha^i}\frac{1}{\beta^{m-i}}.$$

Hence

$$\mathcal{Z}_N = \begin{cases} \displaystyle\sum_{m=1}^{N}\mathtt{B}_{N,m}\frac{\beta^{-m-1}-\alpha^{-m-1}}{\beta^{-1}-\alpha^{-1}} & \alpha\neq\beta, \\ \displaystyle\sum_{m=1}^{N}\mathtt{B}_{N,m}(m+1)\alpha^{-m} & \alpha=\beta. \end{cases} \tag{11}$$

We conclude that by means of formulas (10) and (11), one can enumerate the probability of an arbitrary steady-state configuration of the TASEP.

3. One-dimensional representation of an associated matrix algebra

As demonstrated above, the steady-state probability distribution of an arbitrary arrangement of TASEP particles is derived from the matrix algebra (6)–(8). Such a quadratic algebra is formulated for two matrices D and E which are associated with the particles and holes, respectively. As proven in [27], the matrices fulfilling the rules (6)–(8) are non-commuting and infinity dimensional, in general. However, for the special choice of the parameters α and β, the matrices E and D can be commuting, i.e. $DE = ED$. Under this condition, equation (6) leads to the equations

$$D+E = DE = ED, \qquad \frac{1}{\beta}|v\rangle + E|v\rangle = E|v\rangle\frac{1}{\beta} \tag{12}$$

$$\frac{1}{\beta}\langle w|v\rangle + \frac{1}{\alpha}\langle w|v\rangle = \langle w|v\rangle\frac{1}{\alpha\beta} \qquad \alpha+\beta=1. \tag{13}$$

Thus, if condition (13) is guaranteed, the commuting matrices D and E are one dimensional, i.e. they are represented in fact by the numbers $E=\alpha^{-1}$ and $D=\beta^{-1}$. Consecutively, we can choose $\langle w| = |v\rangle = 1$. Above that, as the partition sum is now reduced to

$$\mathcal{Z}_N = \frac{\langle w|(D+E)^N|v\rangle}{\langle w|v\rangle} = \left(\frac{1}{\alpha\beta}\right)^N,$$

the steady-state probability (for the set of configurations $\mathscr{X}$) reads as

$$\mathrm{P}_{\mathrm{ss}}(\mathscr{X}) = (\alpha\beta)^N\left(\frac{1}{\beta}\right)^{\Sigma n_i}\left(\frac{1}{\alpha}\right)^{\Sigma m_i}\left(\frac{1}{\alpha\beta}\right)^{\Sigma \ell_i} = \alpha^{N-\Sigma m_i-\Sigma\ell_i}\beta^{N-\Sigma n_i-\Sigma\ell_i} = \alpha^{\Sigma n_i}(1-\alpha)^{\Sigma m_i}.$$

4. Macroscopic characteristics in mean-field approximation

For the purpose of this paper, we briefly summarize the known results on the macroscopical behavior of the TASEP model. We concentrate predominantly on the bulk density and flux in mean-field approximation. Specifically, the average density of particles occurring inside the

*i*th cell can be understood as the probability of finding the system in a certain configuration chosen from $\mathscr{X}_{\varrho_i} = (0, 0, i-1, 1, 0, N-i)$. That means

$$\varrho_i^{(N)} = \mathrm{P}_{\mathrm{ss}}(\mathscr{X}_{\varrho_i}) = \frac{\langle w|(D+E)^{i-1}D(D+E)^{N-i}|v\rangle}{\langle w|(D+E)^{N}|v\rangle}\,. \tag{14}$$

Similarly, the flux through the *i*th site is defined as

$$J_i^{(N)} = \mathrm{P}_{\mathrm{ss}}(\mathscr{X}_{J_i}) = \frac{\langle w|(D+E)^{i-1}DE(D+E)^{N-i-1}|v\rangle}{\langle w|(D+E)^{N}|v\rangle} = \frac{\mathcal{Z}_{N-1}}{\mathcal{Z}_N}\,, \tag{15}$$

where $\mathscr{X}_{J_i} = (0, 0, i-1, 1, 1, N-i-1)$. Using the large N approximations

$$\mathcal{Z}_N \approx \begin{cases} \dfrac{\beta\alpha(1-2\alpha)}{\beta-\alpha}\left(\dfrac{1}{\alpha(1-\alpha)}\right)^{N+1} & \alpha < \dfrac{1}{2} \wedge \alpha < \beta, \\ \dfrac{\beta\alpha(1-2\beta)}{\alpha-\beta}\left(\dfrac{1}{\beta(1-\beta)}\right)^{N+1} & \beta < \dfrac{1}{2} \wedge \beta < \alpha, \\ \dfrac{\beta\alpha}{\sqrt{\pi}(\alpha-\beta)}\left[\dfrac{1}{(2\alpha-1)^2} - \dfrac{1}{(2\beta-1)^2}\right]\dfrac{4^N}{N^{3/2}} & \alpha > \dfrac{1}{2} \wedge \beta > \dfrac{1}{2}, \\ \dfrac{\alpha^2}{\sqrt{\pi}(2\alpha-1)^3}\dfrac{4^{N+1}}{N^{3/2}} & \alpha = \beta > \dfrac{1}{2}, \\ \dfrac{(1-2\alpha)^2}{(1-\alpha)^2}\dfrac{N}{\alpha^N(1-\alpha)^N} & \alpha = \beta < \dfrac{1}{2}, \\ \dfrac{2\beta}{\sqrt{\pi}(2\beta-1)}\dfrac{4^N}{N^{1/2}} & \alpha = \dfrac{1}{2} < \beta, \\ 4^N & \alpha = \beta = \dfrac{1}{2} \end{cases} \tag{16}$$

derived in [27], we ascertain that (for an arbitrary cell being far from the boundaries of the system) the relevant bulk density is given by

$$\varrho(\alpha,\beta) = \begin{cases} \frac{1}{2} & \alpha \geqslant \frac{1}{2} \wedge \beta \geqslant \frac{1}{2}, \\ \alpha & \alpha < \frac{1}{2} \wedge \beta > \alpha, \\ 1-\beta & \beta < \frac{1}{2} \wedge \beta < \alpha, \\ \alpha & \alpha + \beta = 1. \end{cases} \tag{17}$$

Regarding the TASEP flux J, it is trivial to show that it is independent of i and

$$J(\alpha,\beta) = \begin{cases} \frac{1}{4} & \alpha \geqslant \frac{1}{2} \wedge \beta \geqslant \frac{1}{2}, \\ \alpha(1-\alpha) & \alpha < \frac{1}{2} \wedge \beta > \alpha, \\ \beta(1-\beta) & \beta < \frac{1}{2} \wedge \beta < \alpha, \\ \alpha\beta & \alpha + \beta = 1. \end{cases} \tag{18}$$

After comparing results (16) and (18), we close this section with the assertion that the fundamental diagram of the TASEP model (see figure 4) is described by the equation

$$J(\varrho) = \varrho(1-\varrho). \tag{19}$$

For completeness, we denote that the region of the parameters α, β delimited in formulas (16)–(18) is used to be divided as follows:

- LD1: low-density region ♯1 ($\alpha < \beta < 1-\alpha$),
- LD2: low-density region ♯2 ($2-2\beta < 2\alpha < 1$),
- MC: maximal-current region ($2\alpha > 1 \wedge 2\beta > 1$),
- HD1: high-density region ♯1 ($\beta < \alpha < 1-\beta$),
- HD2: high-density region ♯2 ($2-2\alpha < 2\beta < 1$).

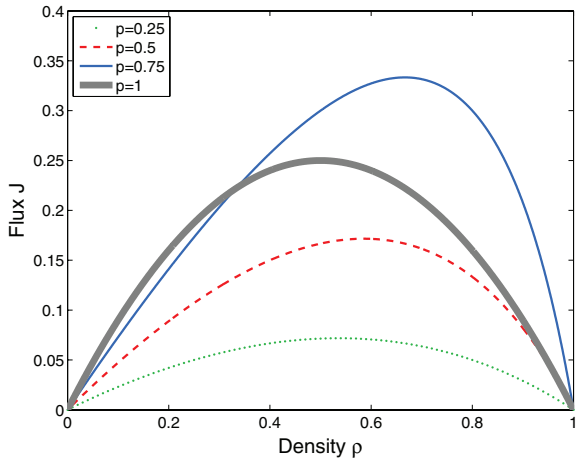

Figure 4. The flow-density relation for the TASEP model. The curves display the function $J = J(\varrho)$ calculated for the ordered-sequential update of the ASEP model with open boundary conditions (for the details on TASEP update-procedures, please see [17]). The parameter p represents the rate for particle transition from the actual cell to the following one. The bold curve displays the theoretical relation (19) valid for the time-continuous TASEP.

5. Distance clearance distribution—a special case

In the main part of this paper, we aim to derive an exact analytical formula for the so-called distance clearance of the TASEP model, i.e. probability density for clear distance (measured in cells) among the subsequent particles of the model. Such a probability density can (in general) depend on the position i of a monitored particle. Hence, the relevant distribution $\wp_i(k)$ depends on i as well. The unnormalized probability of a $(k-1)$cell-gap behind the ith occupied cell is denoted as $\widetilde{\wp}_i(k) = \mathrm{P}_{\mathrm{ss}}(0, 0, i-1, 1, k-1, 0, 1, 0, N-i-k)$ and can be calculated via

$$\widetilde{\wp}_i^{(N)}(k) = \frac{1}{\mathcal{Z}_N} \frac{\langle w|(D+E)^{i-1} D E^{k-1} D (D+E)^{N-i-k}|v\rangle}{\langle w|v\rangle} \qquad (1 \leqslant k \leqslant N-i), \tag{20}$$

because the first $i-1$ cells could be arbitrarily occupied or vacant, the ith cell should be occupied, $k-1$ succeeding cells should be vacant as well, the $(i+k)$th cell should be occupied, and finally the tail of the chain could be occupied/vacant at random. The probability density for clearance is then

$$\wp_i^{(N)}(k) = \mathcal{N} \widetilde{\wp}_i^{(N)}(k),$$

where the constant $\mathcal{N}$ assures the proper normalization computable via the condition

$$\sum_{k=1}^{N-i} \wp_i^{(N)}(k) = 1. \tag{21}$$

If the associated metric algebra is one dimensional, i.e. under condition (13), then equation (20) changes to

$$\wp_i^{(N)}(k) = \mathcal{N} \left(\frac{1}{\alpha}\right)^{N-2} \left(\frac{1}{\beta}\right)^{N+1-k} \qquad (1 \leqslant k \leqslant N-i). \tag{22}$$

The normalization pre-factor $\mathcal{N}$ can be quantified either from condition (21) or the equation

$$\mathcal{N}^{-1} = \frac{\langle w|(D+E)^{i-1}D(D+E)^{N-i}|v\rangle - \langle w|(D+E)^{i-1}DE^{N-i}|v\rangle}{\langle w|v\rangle},$$

which takes into account all possible configurations with the occupied ith cell and rejects those configurations having the empty tail (behind the ith cell), when all the cells $i+1, i+2, \ldots, N$ are vacant. This leads to

$$\mathcal{N}^{-1} = \left(\frac{1}{\alpha}\right)^{N-1}\left(\frac{1}{\beta}\right)^{N}(1-\beta^{N-i}),$$

which yields (if (22) is applied) the desired result

$$\wp_i^{(N)}(k) = \frac{\alpha}{1-\beta^{N-i}}\beta^{k-1}.$$

The large N approximation adjusts such an expression to

$$\wp_i(k) = \lim_{N\to+\infty}\wp_i^{(N)}(k) = \alpha\beta^{k-1}.$$

Note that this result is independent of the cell behind which the clearance is measured. As a consequence, we obtain the formula

$$\langle k\rangle = \sum_{k=1}^{\infty} k\wp_i(k) = \alpha\sum_{k=1}^{\infty} k\beta^{k-1} = \frac{\alpha}{(1-\beta)^2} = \frac{1}{\alpha}$$

for the mean clearance of the TASEP model. If reformulated, the clearance distribution reads as

$$\wp(k) = \varrho(1-\varrho)^{k-1},$$

where the relation $\varrho = \alpha$ is adopted. We remind that these outcomes are valid under the condition $\alpha+\beta = 1$ only.

6. Distance clearance distribution—a general case

To derive the exact formula of $\wp_i^{(N)}(k)$ for an arbitrary choice of parameters α, β, we first rearrange the matrix product in (20) into the form

$$(D+E)^{i-1}DE^{k-1}D(D+E)^{N-i-k} = \sum_{m,n} a_{m,n}E^m D^n.$$

Then, applying rules (7) and (8), the following holds:

$$\langle w|(D+E)^{i-1}DE^{k-1}D(D+E)^{N-i-k}|v\rangle = \sum_{m,n} a_{m,n}\alpha^{-m}\beta^{-n}.$$

Using notation (A.2), lemmas 4 and 5, we obtain (for $k \neq N-i$)

$$\begin{aligned} D(D+E)^{N-i-k} &= \sum_{m=1}^{N-i-k} \mathtt{B}_{N-i-k,m}\sum_{\ell=0}^{m} DE^{\ell}D^{m-\ell} \\ &= \sum_{m=1}^{N-i-k} \mathtt{B}_{N-i-k,m}\sum_{\ell=0}^{m}\left(D^{m-\ell+1} + \sum_{z=1}^{\ell} E^z D^{m-\ell}\right). \end{aligned}$$

Furthermore, by means of lemma 5, we obtain

$$DE^{k-1}D(D+E)^{N-i-k} = \sum_{m=1}^{N-i-k} \mathtt{B}_{N-i-k,m} \sum_{\ell=0}^{m} \left(DE^{k-1}D^{m-\ell+1} + \sum_{z=1}^{\ell} DE^{z+k-1}D^{m-\ell} \right)$$
$$= \sum_{m=1}^{N-i-k} \mathtt{B}_{N-i-k,m} \sum_{\ell=0}^{m} \left(D^{m-\ell+2} + \sum_{w=1}^{k-1} E^w D^{m-\ell+1} + \ell D^{m-\ell+1} + \sum_{z=1}^{\ell} \sum_{w=1}^{z+k-1} E^w D^{m-\ell} \right).$$

For $i \geqslant 2$ we apply lemma 4 to the product $(D+E)^{i-1}$. That provides

$$(D+E)^{i-1}DE^{k-1}D(D+E)^{N-i-k} = \sum_{p=1}^{i-1} \sum_{q=0}^{p} \sum_{m=1}^{N-i-k} \sum_{\ell=0}^{m} \mathtt{B}_{N-i-k,m}\mathtt{B}_{i-1,p} \left(E^q D^{p-q+m-\ell+2} \right.$$
$$\left. + \sum_{w=1}^{k-1} E^q \underbrace{D^{p-q}E^w} D^{m-\ell+1} + \ell E^q D^{p-q+m-\ell+1} + \sum_{z=1}^{\ell} \sum_{w=1}^{z+k-1} E^q \underbrace{D^{p-q}E^w} D^{m-\ell} \right).$$

From lemma 6, we derive that (for $q < p$)

$$D^{p-q}E^w = \sum_{a=1}^{w} \frac{(p-q-a+w-1)!}{(p-q-1)!(w-a)!} E^a + \sum_{b=1}^{p-q} \frac{(p-q-b+w-1)!}{(p-q-b)!(w-1)!} D^b$$
$$= \sum_{a=1}^{w} \mathtt{A}_1 E^a + \sum_{b=1}^{p-q} \mathtt{A}_2 D^b,$$

where we use, for convenience, the notation

$$\mathtt{A}_1 = \frac{(p-q-a+w-1)!}{(p-q-1)!(w-a)!}, \qquad \mathtt{A}_2 = \frac{(p-q-b+w-1)!}{(p-q-b)!(w-1)!}.$$

This leads to the final formula

$$(D+E)^{i-1}DE^{k-1}D(D+E)^{N-i-k}$$
$$= \sum_{p=1}^{i-1} \sum_{m=1}^{N-i-k} \sum_{\ell=0}^{m} \sum_{q=0}^{p-1} \mathtt{B}_{N-i-k,m}\mathtt{B}_{i-1,p} \left(E^q D^{p-q+m-\ell+2} + \ell E^q D^{p-q+m-\ell+1} \right.$$
$$+ \sum_{w=1}^{k-1} \sum_{a=1}^{w} \mathtt{A}_1 E^{q+a} D^{m-\ell+1} + \sum_{w=1}^{k-1} \sum_{a=1}^{p-q} \mathtt{A}_2 E^q D^{m-\ell+1+b} + \sum_{z=1}^{\ell} \sum_{w=1}^{z+k-1} \sum_{a=1}^{w} \mathtt{A}_1 E^{q+a} D^{m-\ell}$$
$$\left. + \sum_{z=1}^{\ell} \sum_{w=1}^{z+k-1} \sum_{b=1}^{p-q} \mathtt{A}_2 E^q D^{m-\ell+b} \right) + \sum_{p=1}^{i-1} \sum_{m=1}^{N-i-k} \sum_{\ell=0}^{m} \mathtt{B}_{N-i-k,m}\mathtt{B}_{i-1,p}$$
$$\times \left(E^p D^{m-\ell+2} + \sum_{w=1}^{k-1} E^{w+p} D^{m-\ell+1} + \ell E^p D^{m-\ell+1} + \sum_{z=1}^{\ell} \sum_{w=1}^{z+k-1} E^{w+p} D^{m-\ell} \right).$$

Multiplying such an expression by the vectors $\langle w|$ and $|v\rangle$ gives the following dependence on the parameters α, β:

$$\wp_i^{(N)}(k) = \frac{\mathcal{N}}{\mathcal{Z}_N \langle w|v\rangle} \sum_{p=1}^{i-1} \sum_{m=1}^{N-i-k} \sum_{\ell=0}^{m} \mathtt{B}_{N-i-k,m}\mathtt{B}_{i-1,p} \left(\frac{1}{\beta}\right)^{m-\ell} \left\{ \left(\frac{1}{\beta^2} + \frac{\ell}{\beta}\right) \sum_{q=0}^{p-1} \left(\frac{1}{\alpha}\right)^q \left(\frac{1}{\beta}\right)^{p-q} \right.$$
$$\left. + \sum_{q=0}^{p-1} \left(\frac{1}{\alpha}\right)^q \sum_{w=1}^{k-1} \frac{1}{\beta} \left(\sum_{a=1}^{w} \mathtt{A}_1 \left(\frac{1}{\alpha}\right)^a + \sum_{b=1}^{p-q} \mathtt{A}_2 \left(\frac{1}{\beta}\right)^b \right) \right.$$

$$+\sum_{z=1}^{\ell}\sum_{q=0}^{p-1}\left(\frac{1}{\alpha}\right)^{q}\sum_{w=1}^{z+k-1}\left(\sum_{a=1}^{w}\mathtt{A}_1\left(\frac{1}{\alpha}\right)^{a}+\sum_{b=1}^{p-q}\mathtt{A}_2\left(\frac{1}{\beta}\right)^{b}\right)$$
$$+\left(\frac{1}{\alpha}\right)^{p}\left(\frac{1}{\beta^2}+\frac{\ell}{\beta}+\sum_{w=1}^{k-1}\left(\frac{1}{\alpha}\right)^{w}\frac{1}{\beta}+\sum_{z=1}^{\ell}\sum_{w=1}^{z+k-1}\left(\frac{1}{\alpha}\right)^{w}\right)\Bigg\}, \tag{23}$$

where we consider $i \geqslant 2$ and $k < N - i$. The formulas for the remaining cases,

$$\wp_1^{(N)}(k)=\frac{\mathcal{N}}{\mathcal{Z}_N\langle w|v\rangle}\sum_{m=1}^{N-i-k}\sum_{\ell=0}^{m}\mathtt{B}_{N-i-k,m}\left(\frac{1}{\beta}\right)^{m-\ell}\left\{\frac{1}{\beta^2}+\frac{\ell}{\beta}+\sum_{w=1}^{k-1}\left(\frac{1}{\alpha}\right)^{w}\frac{1}{\beta}\right.$$
$$\left.+\sum_{z=1}^{\ell}\sum_{w=1}^{z+k-1}\left(\frac{1}{\alpha}\right)^{w}\right\},$$

$$\wp_i^{(N)}(N-i)=\frac{\mathcal{N}}{\mathcal{Z}_N\langle w|v\rangle}\sum_{p=1}^{i-1}\mathtt{B}_{i-1,p}\left\{\sum_{q=0}^{p}\left(\frac{1}{\alpha}\right)^{q}\left(\frac{1}{\beta}\right)^{p-q+1}+\sum_{w=1}^{N-i-1}\left(\frac{1}{\alpha}\right)^{p+w}\right.$$
$$\left.+\sum_{q=0}^{p-1}\left(\frac{1}{\alpha}\right)^{q}\sum_{w=1}^{N-i-1}\left(\sum_{a=1}^{w}\mathtt{A}_1\left(\frac{1}{\alpha}\right)^{a}+\sum_{b=1}^{p-q}\mathtt{A}_2\left(\frac{1}{\beta}\right)^{b}\right)\right\},$$

$$\wp_1^{(N)}(N-1)=\left(\frac{1}{\beta}\right)^{2}+\sum_{w=1}^{N-2}\left(\frac{1}{\alpha}\right)^{w}\left(\frac{1}{\beta}\right),$$

have been obtained analogically.

7. Mean-field versus boundary clearance distribution

Now we focus on the asymptotic clearance distribution $\wp(k)$. As we are interested in the probability of a gap of the length k between two succeeding particles in the bulk (i.e. far from the boundaries) as well as near the boundaries, it is beneficial to fix the position of cells $i, i+1, \ldots, i+k$. Based on this strategy, we denote the number of arbitrary occupied cells before the gap as $m := i - 1$ and the number of arbitrary occupied cells behind the gap by $n := N - i - k$. If investigating the probability of a gap in the bulk, the large N limit is meant in the sense $m, n \to \infty$ proportionally to the lattice size N. On the other hand, if investigating the influence of the right boundary, the number n of particles behind the gap remains fixed (mostly $n = 0$) and the large N limit is meant in the sense $m \to \infty$.

Let us now investigate the behavior of the quantity $\widetilde{\wp}_{m,n}(k) = \widetilde{\wp}_{m+1}^{(N)}(k)$, where $N = m + n + k + 1$. Thus, in terms of the matrix-product-ansatz description (MPA), we focus on

$$\widetilde{\wp}_{m,n}(k)=\frac{1}{\mathcal{Z}_{m+n+k+1}}\frac{\langle w|(D+E)^m DE^{k-1}D(D+E)^n|v\rangle}{\langle w|v\rangle}. \tag{24}$$

Rearranging such a matrix product using (6) for $k = 1$, we obtain

$$(D+E)^m DD(D+E)^n=(D+E)^m D(D+E)^{n+1}-(D+E)^m DE(D+E)^n$$
$$=(D+E)^m D(D+E)^{n+1}-(D+E)^{m+n+1}.$$

And hence, using relations (14) and (15), it holds that

$$\widetilde{\wp}_{m,n}(1)=\varrho_{m+1}^{(n+m+2)}-J^{(n+m+2)}. \tag{25}$$

For $k = 2$, we analogically obtain

$$(D+E)^m DED(D+E)^n = (D+E)^{m+1} D(D+E)^n,$$

and therefore

$$\widetilde{\wp}_{m,n}(2) = \varrho_{m+2}^{(m+n+2)} J^{(m+n+3)}. \tag{26}$$

Moreover, for $k \geqslant 3$ it holds that

$$(D+E)^m DE^{k-1} D(D+E)^n = (D+E)^m DE^{k-2} D(D+E)^n + (D+E)^{m-1} DE^k D(D+E)^n.$$

That leads to the formula

$$\widetilde{\wp}_{m-1,n}(k+1) = \widetilde{\wp}_{m,n}(k) - J^{m+n+k+1} \widetilde{\wp}_{m,n}(k-1). \tag{27}$$

Let us now study such a system in the limit $m \to \infty$. This corresponds with the system on an infinite half-line with the right boundary open. We will now fix the number n of arbitrary occupied cells behind the gap of length k and derive the formulas for $\widetilde{\wp}_n(k) := \lim_{m\to\infty} \widetilde{\wp}_{m,n}(k)$. Denoting

$$\varrho_{N-(n+a-b)} := \lim_{m\to\infty} \varrho_{m+b}^{(m+n+a)}$$

(see also (14)) and using the asymptotic form of fundamental dependence (19), equations (25)–(27) turn to

$$\widetilde{\wp}_n(1) = \varrho_{N-n-1} - \varrho(1-\varrho), \qquad \widetilde{\wp}_n(2) = \varrho_{N-n}\varrho(1-\varrho), \tag{28}$$

$$\widetilde{\wp}_n(k+1) = \widetilde{\wp}_n(k) - \varrho(1-\varrho)\widetilde{\wp}_n(k-1), \tag{29}$$

where $\varrho = \varrho(\alpha, \beta)$ is the bulk density. The general solution of the recursion equation (29) is of the form

$$\widetilde{\wp}_n(k) = \begin{cases} \mathtt{C}_1\varrho^k + \mathtt{C}_2(1-\varrho)^k & \varrho \neq \dfrac{1}{2}, \\ \dfrac{\mathtt{C}_3}{2^k} + k\dfrac{\mathtt{C}_4}{2^k} & \varrho = \dfrac{1}{2}, \end{cases}$$

where $\mathtt{C}_1, \mathtt{C}_2, \mathtt{C}_3, \mathtt{C}_4$ are to be determined from the initial conditions (28).

In this paper, we are interested in two special cases: (1) $n \to \infty$ (infinite line), (2) $n = 0$ (the leading particle sitting in the right boundary cell). In the first instance, let us investigate the bulk behavior. Denoting

$$\widetilde{\wp}(k) := \lim_{n\to\infty} \widetilde{\wp}_n(k) = \lim_{m,n\to\infty} \widetilde{\wp}_{m,n}(k),$$

the initial conditions (28) turn to $\widetilde{\wp}(1) = \varrho^2$, $\widetilde{\wp}(2) = \varrho^2(1-\varrho)$ and therefore (using the recursion formula (29)) the general solution for $n \to \infty$ reads

$$\widetilde{\wp}(k) = \varrho^2(1-\varrho)^{k-1}. \tag{30}$$

The existence of the limit $\widetilde{\wp}(k)$ for all $k \in \mathbb{N}$ can be elementarily confirmed using mathematical induction by means of relations (25)–(27). The normalization constant $\mathcal{N}$ is then

$$\mathcal{N} = \left(\sum_{k=1}^{\infty} \varrho^2(1-\varrho)^{k-1}\right)^{-1} = \frac{1}{\varrho}$$

and hence the clearance distribution $\wp(k) = \mathcal{N}\widetilde{\wp}(k)$ fulfills the relationship

$$\wp(k) = \varrho(1-\varrho)^{k-1}. \tag{31}$$

All the time we keep in mind that the bulk density ϱ is a function of the parameters α, β given by (17). Thus, the dependence of the clearance distribution (in the bulk) on these parameters reads

$$\wp(k;\alpha,\beta)=\begin{cases}\frac{1}{2^k} & \alpha\geqslant\frac{1}{2}\wedge\beta\geqslant\frac{1}{2},\\ \alpha(1-\alpha)^{k-1} & \alpha<\frac{1}{2}\wedge\beta>\alpha,\\ (1-\beta)\beta^{k-1} & \beta<\frac{1}{2}\wedge\beta<\alpha,\\ \alpha\beta^{k-1} & \alpha+\beta=1.\end{cases}$$

The relevant evaluation of this outcome is visualized in figures 7–11. These figures show the clearance distribution $\wp_i^{(N)}(k)$ calculated via the exact formula (23) and the large N approximation $\wp(k)$ calculated via (31). They are organized as follows. Plots 7, 8, 9, 10, and 11 correspond to the phases LD1 (low-density regime ♯1), LD2 (low-density regime ♯2), MC (maximal-current regime), HD1 (high-density regime ♯1), and HD2 (high-density regime ♯2), respectively. The individual subplots demonstrate the influences of the lattice length, i.e. they show the way how the distribution $\wp_i^{(N)}(k)$ converges to the asymptotic curve (31). Also, discrepancies between (23) and (31) may be explained using the corresponding density profiles $\varrho_i^{(N)}$ figured under these subplots.

Now we concentrate on the netto-gap distribution near the right-hand tail of the lattice, i.e. we consider $n=0$. In this case, the initial conditions will be derived from formula (14). It is easy to verify that

$$\varrho_{N-0}=\frac{\varrho(1-\varrho)}{\beta}\quad\text{and}\quad\varrho_{N-1}=\frac{\varrho^2(1-\varrho)^2}{\beta^2}+\varrho(1-\varrho).$$

Hence, the initial conditions have the form

$$\widetilde{\wp}_0(1)=\frac{\varrho^2(1-\varrho)^2}{\beta^2}\quad\text{and}\quad\widetilde{\wp}_0(2)=\frac{\varrho^2(1-\varrho)^2}{\beta}.$$

The particular solution then reads

$$\widetilde{\wp}_0(k;\alpha,\beta)=\begin{cases}\dfrac{1}{\beta^2 2^{k+2}}\left(1-\dfrac{k}{2}+\beta(k-1)\right) & \alpha\geqslant\dfrac{1}{2}\wedge\beta\geqslant\dfrac{1}{2},\\ \dfrac{\alpha^2(1-\alpha)^{k+1}}{\beta^2}\left(\dfrac{\beta-\alpha}{1-2\alpha}\right)+\dfrac{\alpha^{k+1}(1-\alpha)^2}{\beta^2}\left(1-\dfrac{\beta-\alpha}{1-2\alpha}\right) & \alpha<\dfrac{1}{2}\wedge\beta>\alpha,\\ (1-\beta)^2\beta^{k-1} & \beta<\dfrac{1}{2}\wedge\beta<\alpha,\\ \alpha^2\beta^{k-1} & \alpha+\beta=1.\end{cases}\tag{32}$$

After normalization $\mathcal{N}=\left(\sum_{k\in\mathbb{N}}\widetilde{\wp}_0(k)\right)^{-1}=\varrho_{N-0}^{-1}=\frac{\beta}{\varrho(1-\varrho)}$, the probability density for gap k between particles being close to the right boundary is

$$\wp_0(k;\alpha,\beta)=\begin{cases}\dfrac{1}{\beta 2^k}\left(1-\dfrac{k}{2}+\beta(k-1)\right) & \alpha\geqslant\frac{1}{2}\wedge\beta\geqslant\dfrac{1}{2},\\ \dfrac{\alpha(1-\alpha)^k}{\beta}\left(\dfrac{\beta-\alpha}{1-2\alpha}\right)+\dfrac{\alpha^k(1-\alpha)}{\beta}\left(1-\dfrac{\beta-\alpha}{1-2\alpha}\right) & \alpha<\dfrac{1}{2}\wedge\beta>\alpha,\\ (1-\beta)\beta^{k-1} & \beta<\dfrac{1}{2}\wedge\beta<\alpha,\\ \alpha\beta^{k-1} & \alpha+\beta=1.\end{cases}\tag{33}$$

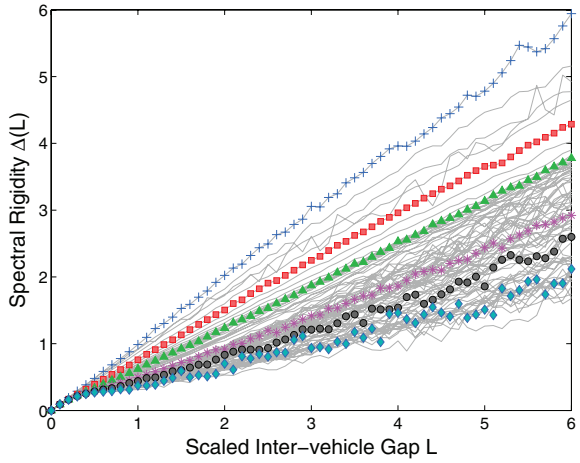

Figure 5. Spectral rigidity of vehicular traffic. The gray curves correspond to the rigidity $\Delta(L)$ analyzed separately in 85 density regions. The chosen results of relevant statistical analysis are picked out. Specifically, the plus signs, squares, triangles, stars, circles, and diamonds represent the rigidities obtained for traffic data from the following density regions: [2,3), [6,7), [16,17), [26,27), [40,41), and [85,86) vehicles/km/lane, respectively. For details, please see [25].

By means of computer simulations, one can see that the asymptotic values (33) are in very good agreement with numerical implementation of the model even for small-sized lattices. In figure 12, we can see the comparison of simulation results for $N = 20$ (bullets and plus signs) with the analytical values (33) (dashed and dash-dotted lines) together with the bulk prediction $\wp(k) = \varrho(1-\varrho)^{k-1}$ (bold continuous line).

8. Mean-field spectral rigidity of the TASEP model

Description of traffic microstructure by means of the inter-vehicle gap distribution $\wp(r)$ is, as discussed above, usual in traffic theory. However, clearance distribution depicts the distance gaps between two successive vehicles only. Aiming to investigate the middle-ranged interactions among the cars, it is necessary to find a mathematical quantity suitable for quantifying the level of synchronization for larger clusters of particles. This desired quantity can be found in random matrix theory (see [30]) where it provides an insight into the structure of the eigenvalues of random matrix ensembles. It is called *a spectral rigidity.* If reformulated within the bounds of traffic theory, the spectral rigidity has the following interpretation.

Consider a set $\{r_i : i = 1 \dots Q\}$ of netto gaps between each pair of the succeeding cars moving on a one-lane freeway. We suppose that the mean gap taken over the complete set is re-scaled to 1, i.e.

$$\sum_{i=1}^{Q} r_i = Q. \tag{34}$$

Dividing the interval $[0, Q)$ into subintervals $\big[(k-1)L, kL\big)$ of length L and denoting by $n_k(L)$ the number of cars in the kth subinterval, the average value $\overline{n}(L)$ taken over all possible subintervals is

$$\overline{n}(L) = \frac{1}{\lfloor Q/L \rfloor} \sum_{k=1}^{\lfloor Q/L \rfloor} n_k(L) = L,$$

where the integer part $\lfloor Q/L \rfloor$ stands for the number of all subintervals $\big[(k-1)L, kL\big)$ included in the entire interval $[0, Q)$. We suppose, for convenience, that Q/L is integer, i.e. $\lfloor Q/L \rfloor = Q/L$. The spectral rigidity $\Delta(L)$ is then defined as

$$\Delta(L) = \frac{L}{Q} \sum_{k=1}^{Q/L} \big(n_k(L) - L\big)^2$$

and represents the statistical variance of the number of vehicles moving at the same time inside a fixed part of the road of length L. For the one-parametric family of distributions (1), it was proved in [25] that the associated spectral rigidity has a form

$$\Delta(L) = \chi L + \gamma + \mathcal{O}(L^{-1}), \tag{35}$$

where (together with relation (2))

$$\chi = \chi(\nu) = \frac{2 + \sqrt{B\nu}}{2B(1 + \sqrt{B\nu})} \tag{36}$$

and

$$\gamma = \gamma(\nu) = \frac{6\sqrt{B\nu} + B\nu\big(21 + 4B\nu + 16\sqrt{B\nu}\big)}{24\big(1 + \sqrt{B\nu}\big)^4}. \tag{37}$$

We recall that the parameter ν reflects the inverse temperature of the traffic gas and the constant $B = B(\nu)$ is derived from relation (2). Equation (35) prognosticates that the rigidity is a linear function whose slope χ is depending on the mental strain coefficient ν (briefly described in section 1). Approximately, the changes of χ (with respect to the traffic density) can be described as follows. For small densities, the slope χ in the relation $\Delta(L) \approx \chi L + \gamma$ is close to 1 as expected for statistically independent events. Nevertheless, if the traffic density increases, the interactions among vehicles strengthen, which results in a descent of the slope χ. The more detailed insight into the realistic behavior of $\Delta(L)$ is demonstrated in figure 5, where the experimental results of 'traffic spectral analysis' are plotted.

At the moment, our immediate goal is to derive the analytical formula for the spectral rigidity Δ of the totally asymmetric simple exclusion model. Firstly, note that the mean clearance calculated for distribution (31) is

$$\langle k \rangle = \sum_{k=1}^{\infty} k\varrho(1-\varrho)^{k-1} = \frac{1}{\varrho},$$

which means that at the end of our computations there will be necessity to revise the results in accord with the general definition (34). Now, denote by $n_\ell(s)$ the probability that there is exactly s particles inside the fixed ℓ-cells region of the TASEP chain. As understandable, such a probability reads

$$n_\ell(s) = \binom{\ell}{s} \varrho^s (1-\varrho)^{\ell - s} \quad (s = 0, 1, \ldots, \ell).$$

Since

$$\langle s \rangle = \sum_{s=0}^{\ell} \frac{\ell!}{(\ell - s)!(s-1)!} \varrho^s (1-\varrho)^{\ell - s} = \varrho\ell$$

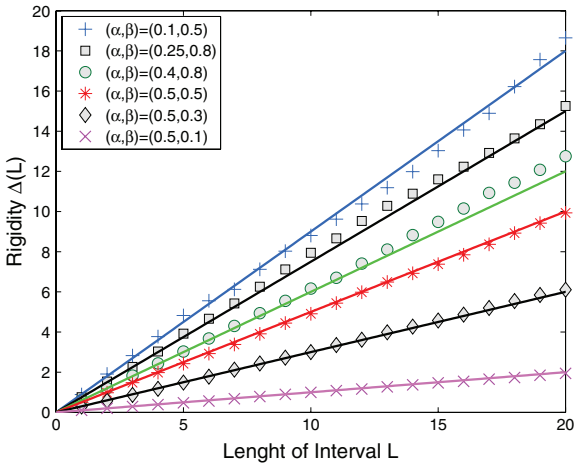

Figure 6. Spectral rigidity of the TASEP model. The signs represent the numerically-obtained spectral rigidity $\Delta(L)$ for the TASEP with parameters α, β indicated in the legend. The curves display the corresponding rigidity calculated via the exactly-derived formula (38).

and

$$\langle s^2\rangle = \sum_{s=0}^{\ell} \frac{s\ell!}{(\ell-s)!(s-1)!}\varrho^s(1-\varrho)^{\ell-s} = \varrho\ell\big(1+\varrho(\ell-1)\big),$$

the corresponding statistical variance is of a form

$$\sigma^2 = \langle s^2\rangle - \langle s\rangle^2 = \varrho\ell(1-\varrho),$$

which leads (after the transition to the re-scaled headways $L = \varrho\ell$) to the final formula for the spectral rigidity

$$\Delta(L) = (1-\varrho)L. \tag{38}$$

Obviously, the slope $\chi = 1-\varrho$ of the rigidity $\Delta(L)$ decreases linearly with increasing density of the TASEP particles, as confirmed by the numerous numerical tests visualized in figure 6. This result is very similar to the behavior revealed in realistic traffic samples.

9. Summary and conclusions

Using the MPA formalism, we have derived the general analytical formula (23) for distance clearances among the subsequent particles of the TASEP model with open boundaries. Such an exact formula has been substantially simplified for the middle segment of sufficiently long TASEP chains (see (31)). The general formula (23) as well as the bulk simplification (31) have been consecutively compared to the numerical representation of the TASEP model. The discrepancies between these relationships have been detected for small-sized systems only, where the boundary effects strongly influence the movements of all internal particles. However, the generality of formula (23) for clearances measured in an arbitrary part of the lattice has been confirmed also for the boundary tail of the system. Here we have compared numerical results with the analytical formula (23) and found excellent agreement, affirming the correctness of the presented results. In contrast, if the boundary clearances are compared to the bulk prediction (31), we detect substantial incompatibility. This can be explained by the

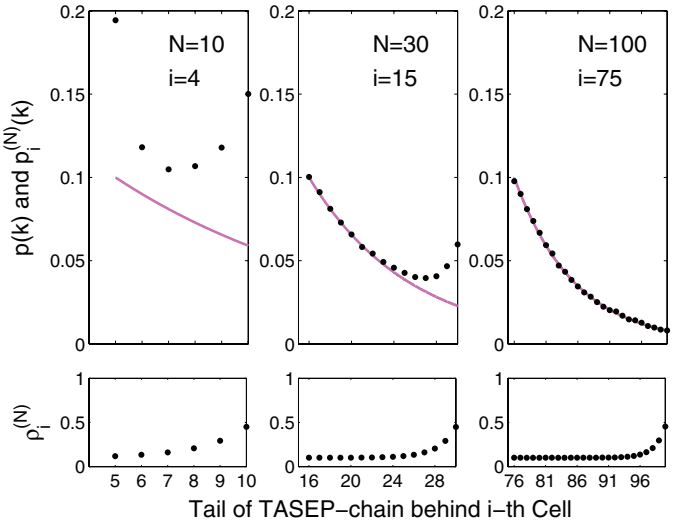

Figure 7. Clearance distribution in the phase of low density ♯1. We plot the inter-particle distance distribution calculated for the TASEP with $\alpha = 0.1$ and $\beta = 0.2$. The bullets visualize the clearance distribution $\wp_i^{(N)}(k)$ enumerated via the exact formula (23), while continuous curves visualize the large N approximations $\wp(k)$ summarized by relation (31). Above that, we also plot the relevant densities, which synoptically illustrates the reasons for discrepancies between (23) and (31).

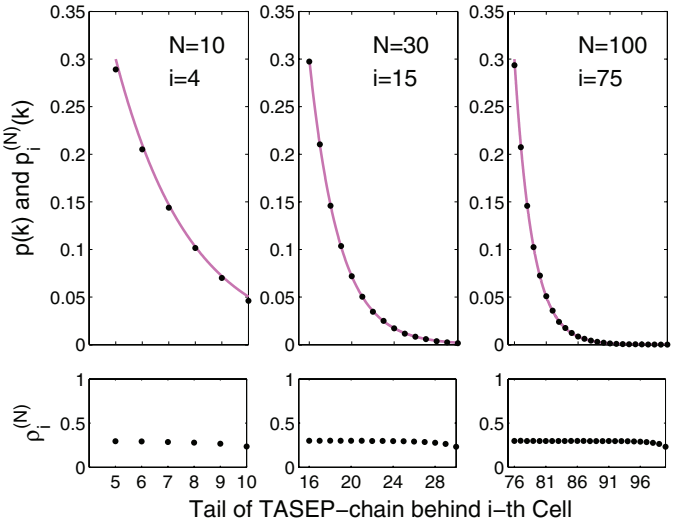

Figure 8. Clearance distribution in the phase of low density ♯2. We plot the inter-particle distance distribution calculated for the TASEP with $\alpha = 0.3$ and $\beta = 0.9$.

fact that the boundary conditions for particle movements are completely different from those stated for the inside of the system.

If the TASEP clearances are compared to the empirically-obtained clearance distributions of vehicular streams, one can see two different situations. Comparing the TASEP and

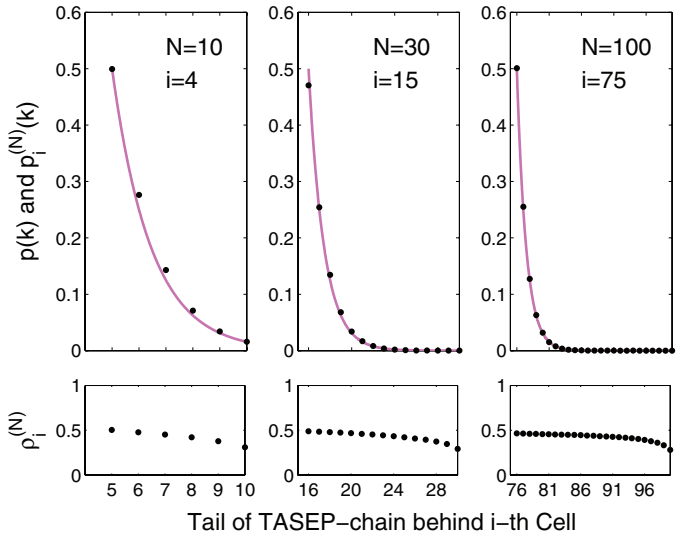

Figure 9. Clearance distribution in the phase of maximum current. We plot the inter-particle distance distribution calculated for the TASEP with $\alpha = 0.8$ and $\beta = 0.9$.

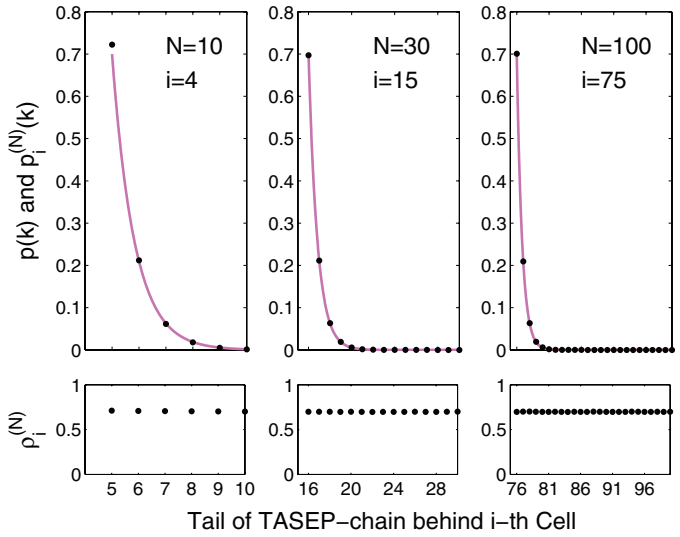

Figure 10. Clearance distribution in the phase of high density ♯1. We plot the inter-particle distance distribution calculated for the TASEP with $\alpha = 0.9$ and $\beta = 0.3$.

real-road traffic for small densities of elements, we uncover the comparatively similar behavior. Specifically, if the relevant clearances are re-scaled to mean clearance equal to 1, both systems show the same asymptotic clearance distribution $\wp(r) = \Theta(r)\mathrm{e}^{-r}$. Such a behavior is exceptable because of weak interactions in the systems mentioned. Completely different situations can be detected for high densities. Whereas the TASEP clearances are still exponentially-distributed (which can be simply substantiated by the knowledge that on the

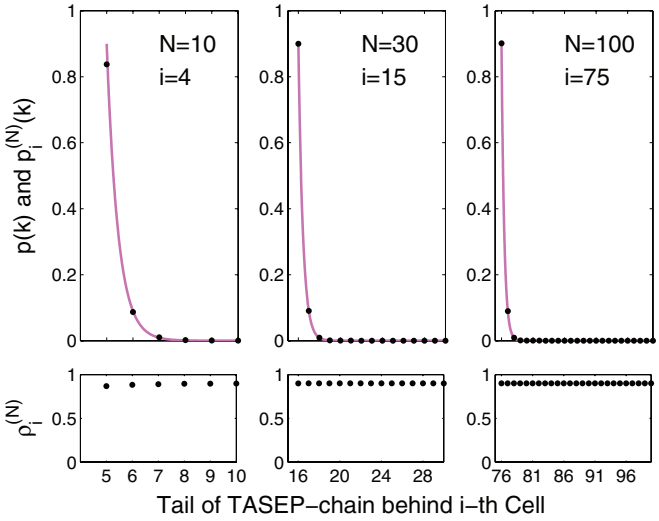

Figure 11. Clearance distribution in the phase of high density ♯2. We plot the inter-particle distance distribution calculated for the TASEP with $\alpha = 0.2$ and $\beta = 0.1$.

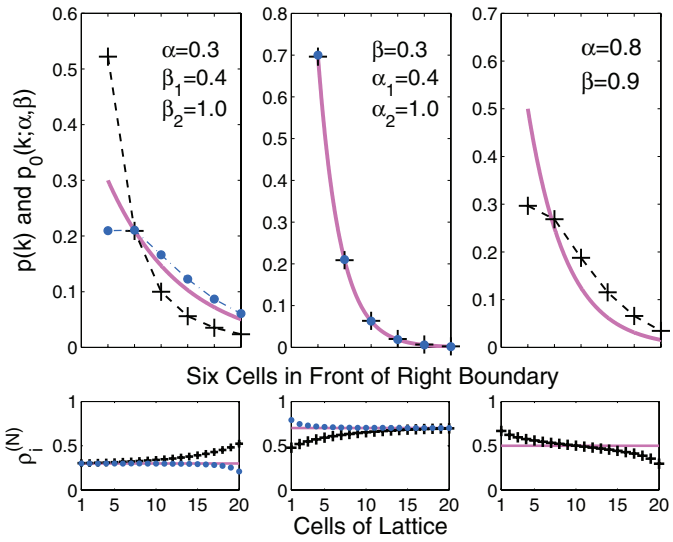

Figure 12. Clearance distribution near the right boundary. The inter-particle distribution (33) is plotted for $N = 20$ particles in three phases LD, HD, and MC together with the corresponding density profiles. In the left graph (LD), we may compare the values (32) (dashed line for β_1 and dash-and-dotted line for β_2) with simulation results (plus signs for β_1 and bullets for β_2) and asymptotic curve (31) (continuous curve). The outputs of numerical simulations for the HD regime (middle subplot) are visualized by the plus signs (for α_1) and bullets (for α_2). In this case, the corresponding curves (32) coincide with the bulk prediction (31) (continuous curve). The plot for the maximum-current phase (right) is structured analogically.

infinite lattice the Bernoulli measure is stationary), the high-density traffic distributions $\wp(r)$ show marked descent for occurrences of small gaps, i.e. $\lim_{r\to 0_+} \wp(r) = 0$. The reason for

such a discrepancy is hidden predominantly in the fact that car correlations in the vehicular traffic are middle-ranged, which means that in relatively dense traffic the cars interact in more extensive clusters. Here the phase of traffic congestion leads to strong car repulsion, which results in small probability for two vehicles being close to each other (with respect to the mean distance between two successive cars). Similar effects cannot be detected among TASEP particles since the TASEP repulsion is strictly hard-cored.

On the other hand, if the spectral rigidities $\Delta(L)$ are compared, both systems generate very similar dependence on the length L of the road. This unexpected similarity is probably a consequence of the different nature of systems analyzed. Anyway, whereas vehicular traffic is a space-continuous system, the TASEP model is cellular system whose elements can occur in the prescribed positions only. This discrete nature brings certain additional interactions into the system observed, which subsequently projects onto the rigidity analysis.

To conclude, although in some aspects the TASEP model and real-road vehicular traffic show similar signs in relevant microstructure, the cellular model TASEP seems to be suitable for macroscopical traffic simulations only. This well-known result is now confirmed by detailed analysis of TASEP microstructure. However, that analysis itself is very contributive because it reveals the detailed changes of particle distributions inside the lattice as well as near the boundaries. Up to the present time, no similar investigation has been realized.

Acknowledgments

The authors would like to thank Bogolyubov Laboratory of Theoretical Physics, Joint Institute of Nuclear Research in Dubna (Russia) for incentives to the presented research. This work was supported by the Ministry of Education, Youth and Sports of the Czech Republic within the project MSM 6840770039.

Appendix

Lemma 1. *Let m, n, a be the arbitrary natural numbers. Let $a \leqslant m$. Then*

$$\sum_{i=a}^{m} \binom{n-i+m-1}{n-1} = \binom{n+m-a}{n}. \tag{A.1}$$

Proof. We will proceed using the mathematical induction. Let $m = a = 1$. Then for an arbitrary $n \in \mathbb{N}$,

$$\sum_{i=1}^{1} \binom{n-i}{n-1} = \binom{n-1}{n-1} = \binom{n}{n}.$$

Now let relation (A.1) hold for all $a \leqslant m$. Then for $a < m+1$,

$$\sum_{i=a}^{m+1} \binom{n-i+m}{n-1} = \sum_{i=a}^{m} \binom{n-i+m-1}{n-1} + \binom{n-a+m}{n-1} = \binom{n+m-a}{n} + \binom{n-a+m}{n-1}$$
$$= \binom{n-a+m+1}{n}.$$

The case $a = m+1$ can be proven analogically to the case $m = 1, a = 1$. □

Lemma 2. *If using the notation*

$$\mathtt{B}_{n,p} = \begin{cases} \dfrac{p(2n-p-1)!}{n!(n-p)!} & 0 < p \leqslant n, \\ 0 & \text{otherwise}, \end{cases} \tag{A.2}$$

it can simply be verified that for $n > 0$ and $p \geqslant 0$,

$$\mathtt{B}_{n,p} = \mathtt{B}_{n+1,p+1} - \mathtt{B}_{n+1,p+2}.$$

Lemma 3. *For the arbitrary square matrices D, E fulfilling $DE = D + E$ and for $n \geqslant 0$,*

$$D^n(D+E) = D^{n+1} + D^{n-1}(D+E) = \sum_{q=1}^{n+1} D^q + E.$$

Lemma 4. *Assume D, E to be arbitrary square matrices fulfilling the relation $DE = D+E$. Let n be the natural number. Then*

$$(D+E)^n = \sum_{m=1}^{n} \mathtt{B}_{n,m} \sum_{q=0}^{m} E^q D^{m-q}. \tag{A.3}$$

Proof. Again, we will use the mathematical induction with respect to n. Let us assume that (A.3) holds. Then with the help of lemmas 2 and 3, we elementarily deduce that

$$\begin{aligned}(D+E)^{n+1} &= \sum_{m=1}^{n} \mathtt{B}_{n,m} \sum_{q=0}^{m} E^q D^{m-q}(D+E) = \sum_{m=1}^{n} \mathtt{B}_{n+1,m+1} \sum_{q=0}^{m} \left(E^{q+1} + E^q \sum_{p=1}^{m-q+1} D^q \right) \\ &\quad - \sum_{m=1}^{n} \mathtt{B}_{n+1,m+2} \sum_{q=0}^{m} \left(E^{q+1} + E^q \sum_{p=1}^{m-q+1} D^q \right) \\ &= \mathtt{B}_{n+2,2}(D+E)^2 + \sum_{m=3}^{n+1} \mathtt{B}_{n+1,m} \sum_{q=0}^{m} E^q D^{m-q} = \sum_{m=1}^{n+1} \mathtt{B}_{n+1,m} \sum_{q=0}^{m} E^q D^{m-q}. \end{aligned}$$

□

Lemma 5. *Assume D, E to be arbitrary square matrices fulfilling the relation $DE = D+E$. Let $n \in \mathbb{N}$. Then*

$$DE^n = DE^{n-1} + E^n = D + \sum_{w=1}^{n} E^w. \tag{A.4}$$

Lemma 6. *Assume D, E to be arbitrary square matrices fulfilling the relation $DE = D+E$. Let m, n be the natural numbers. Then*

$$D^n E^m = \sum_{i=1}^{m} \binom{n-i+m-1}{n-1} E^i + \sum_{j=1}^{n} \binom{n-j+m-1}{m-1} D^j. \tag{A.5}$$

Proof. We will use the mathematical induction. For $n = 1$ and an arbitrary $m \in \mathbb{N}$, expression (A.5) reduces to expression (A.4). Let us now assume that (A.5) holds true for

some $n \in \mathbb{N}$. By means of lemmas 1 and 5, we obtain

$$D(D^n E^m) = \sum_{i=1}^{m} \binom{n-i+m-1}{n-1} \left[D + \sum_{w=1}^{i} E^w \right] + \sum_{j=1}^{n} \binom{n-j+m-1}{m-1} D^{j+1}$$

$$= \sum_{j=1}^{n+1} \binom{n-j+m}{m-1} D^j + \sum_{w=1}^{m} E^w \sum_{i=w}^{m} \binom{n-i+m-1}{n-1} = \sum_{i=1}^{m} \binom{n-i+m}{n} E^i$$

$$+ \sum_{j=1}^{n+1} \binom{n-j+m}{m-1} D^j. \qquad \square$$

References

[1] Schütz G M and Tang L H 1997 *Int. J. Mod. Phys.* B **11** 197
[2] Shaw L B, Zia R K P and Lee K L 2003 *Phys. Rev.* E **68** 021910
[3] Krug J and Tang L H 1994 *Phys. Rev.* E **50** 104
[4] Janowsky S A and Lebowitz J L 1992 *Phys. Rev.* A **45** 618
[5] Schütz G M 1993 *J. Stat. Phys.* **71** 471
[6] Derrida B, Janowsky S A, Lebowitz J L and Speer E R 1993 *Europhys. Lett.* **22** 651
[7] Mallick K 1996 *J. Phys. A: Math. Gen.* **29** 5375
[8] Barkema G T, Marko J F and Widom B 1994 *Phys. Rev.* E **49** 5303
[9] Waterman M S 1995 *Introduction to Computational Biology: Maps, Sequences and Genomes* (*Interdisciplinary Statistics*) (London: Chapman and Hall)
[10] Schreckenberg M, Schadschneider A, Nagel K and Ito N 1995 *Phys. Rev.* E **51** 2939
[11] Ha M, Timonen J and den Nijs M 2003 *Phys. Rev.* E **68** 056122
[12] Chowdhury D, Pasupathy A and Sinha S 1998 *Eur. Phys. J.* B **5** 781
[13] Fouladvand M E and Neek-Amali M 2007 *Europhys. Lett.* **80** 60002
[14] Antal T and Schütz G M 2000 *Phys. Rev.* E **62** 83
[15] Helbing D 2001 *Rev. Mod. Phys.* **73** 1067
[16] Chowdhury D, Santen L and Schadschneider A 2000 *Phys. Rep.* **329** 199
[17] Rajewsky N, Santen L, Schadschneider A and Schreckenberg M 1998 *J. Stat. Phys.* **92** 151
[18] Krbálek M 2008 *J. Phys. A: Math. Theor.* **41** 205004
[19] Abul-Magd A Y 2007 *Phys. Rev.* E **76** 057101
[20] Appert-Rolland C 2009 *Phys. Rev.* E **80** 036102
[21] Treiber M, Kesting A and Helbing D 2006 *Phys. Rev.* E **74** 016123
[22] Krbálek M 2007 *J. Phys. A: Math. Theor.* **40** 5813
[23] Krbálek M, Šeba P and Wagner P 2001 *Phys. Rev.* E **64** 066119
[24] Treiber M and Helbing D 2009 *Eur. Phys. J.* B **68** 607
[25] Krbálek M and Šeba P 2009 *J. Phys. A: Math. Theor.* **42** 345001
[26] Derrida B 1998 *Phys. Rep.* **301** 65
[27] Derrida B, Evans M R, Hakim W and Pasquier V 1993 *J. Phys. A: Math. Gen.* **26** 1493
[28] Derrida B and Evans M R 1997 *Non-equilibrium Statistical Mechanics in One Dimension* (Cambridge: Cambridge University Press) p 277
[29] Blythe R A and Evans M R 2007 *J. Phys. A: Math. Theor.* **40** R333
[30] Mehta M L 1991 *Random Matrices (revised and enlarged)* (New York: Academic)